Generation of a Sleeping Beauty Transposon-Based Cellular System for Rapid and Sensitive Screening for Compounds and Cellular Factors Limiting SARS-CoV-2 Replication

Marek Widera[1]*, Alexander Wilhelm[1,2], Tuna Toptan[1], Johanna M. Raffel[1], Eric Kowarz[2], Fabian Roesmann[1], Finn Grözinger[1], Anna Lena Siemund[2], Vanessa Luciano[2], Marius Külp[2], Jennifer Reis[2], Silvia Bracharz[2], Christiane Pallas[1], Sandra Ciesek[1,3,4†] and Rolf Marschalek[2†]

[1] Institute for Medical Virology, University Hospital Frankfurt am Main, Goethe University, Frankfurt am Main, Germany, [2] Institute of Pharmaceutical Biology, Goethe University, Frankfurt am Main, Germany, [3] German Center for Infection Research, Braunschweig, Germany, [4] Fraunhofer Institute for Molecular Biology and Applied Ecology, Branch Translational Medicine and Pharmacology, Frankfurt am Main, Germany

The severe acute respiratory syndrome coronavirus 2 (SARS-CoV-2) is the causative agent of the acute respiratory disease COVID-19, which has become a global concern due to its rapid spread. The common methods to monitor and quantitate SARS-CoV-2 infectivity in cell culture are so far time-consuming and labor-intensive. Using the Sleeping Beauty transposase system, we generated a robust and versatile cellular infection model that allows SARS-CoV-2 infection experiments compatible for high-throughput and live cell imaging. The model is based on lung derived A549 cells, which show a profound interferon response and convenient cell culture characteristics. ACE2 and TMPRSS2 were introduced for constitutive expression (A549-AT). Subclones with varying levels of ACE2/TMPRSS2 were screened for optimal SARS-CoV-2 susceptibility. Furthermore, extensive evaluation demonstrated that SARS-CoV-2 infected A549-AT cells were distinguishable from mock-infected cells and already showed approximately 12 h post infection a clear signal to noise ratio in terms of cell roughness, fluorescence and a profound visible cytopathic effect. Moreover, due to the high transfection efficiency and proliferation capacity, Sleeping Beauty transposase-based overexpression cell lines with a second inducible fluorescence reporter cassette (eGFP) can be generated in a very short time, enabling the investigation of host and restriction factors in a doxycycline-inducible manner. Thus, the novel model cell line allows rapid and sensitive monitoring of SARS-CoV-2 infection and the screening for host factors essential for viral replication.

Keywords: SARS-CoV-2, COVID-19, corona virus, high throughput, drug screening, CPE, infection model, live cell imaging

HIGHLIGHTS

- Sleeping Beauty transposon-based cellular system was used to generate a highly susceptible cell line for monitoring SARS-CoV-2 infection.
- The versatile model cell line A549-AT is suitable for rapid and sensitive high-throughput assays.
- Additional gene specific expression cassettes allow the screening for compounds and cellular factors limiting SARS-CoV-2 replication.

INTRODUCTION

The coronavirus disease 2019 (COVID-19) is caused by an infection with the severe acute respiratory syndrome coronavirus 2 (SARS-CoV-2). The origin of SARS-CoV-2 outbreak was initially described in Wuhan, China (Zhu et al., 2020) and rapidly established a worldwide pandemic. Globally, over 175 million cases and 3.79 million deaths in total since the start of the pandemic have been reported by the WHO as published on June 15th, 2021 (World Health Organisation [WHO], 2021).

Severe acute respiratory syndrome coronavirus 2 is a spherical beta coronavirus with a size of 120 nm in diameter, which has a lipid envelope. Viral cell entry depends on the host receptor carboxypeptidase angiotensin I converting enzyme 2 (ACE2) and the cellular transmembrane protease, serine 2 (TMPRSS2) for the priming of the viral glycoprotein (Hoffmann et al., 2020b; Rahman et al., 2020). ACE2 was already identified a functional receptor for SARS-CoV (Li et al., 2003) and physiologically plays a key role in the renin-angiotensin aldosterone system by its ability to degrade angiotensin II to the metabolites angiotensin 1–7 and 1–9 (Keidar et al., 2007; McKinney et al., 2014). The spike glycoproteins (S) of SARS-CoV and SARS-CoV-2 receptor-binding domain (RBD) bind to the ACE2 receptor (Lan et al., 2020). Albeit SARS-CoV-2 RBD was shown to have a higher ACE2 binding affinity compared to SARS-CoV RBD, the entire SARS-CoV-2 S binding affinity is not higher when compared to SARS-CoV, suggesting that SARS-CoV-2 RBD, albeit more potent, is less exposed than SARS-CoV RBD (Shang et al., 2020; Wang Q. et al., 2020).

Activation of the S protein and viral entry is further mediated via sequential proteolytic cleavage by TMPRSS2 enabling the glycoprotein mediated membrane fusion of the viral envelope with the host cell membrane (Belouzard et al., 2009; Heurich et al., 2014). Of note, cells infected with SARS-CoV, MERS-CoV, or SARS-CoV-2 were shown to express S protein on the cell surface and are able to induce syncytia and the formation of a morphological cytopathic effect (CPE) (Matsuyama et al., 2010; Chan et al., 2013; Qian et al., 2013; Buchrieser et al., 2020; Bussani et al., 2020; Hoffmann et al., 2020a). Furthermore, TMPRSS2 was shown to facilitate and accelerate syncytia formation by promoting the fusion process (Buchrieser et al., 2020).

After entry, the viral genomic RNA (vRNA), which serves as a template for initial polyprotein translation and generation of non-structural proteins 1–16 (NSP1–16), is subjected to complementary transcription catalyzed by the viral RNA dependent RNA-polymerase (RdRP). In addition, the full genomic repertoire is expanded by the usage of a process named discontinuous transcription in which subgenomic RNAs (sgRNAs) are formed (Kim et al., 2020) serving as templates for the translation of downstream ORFs 3a-9b, including the E, M, and N genes. SgRNAs are each composed of an RNA primer that can co-transcriptionally jump to sequences at transcription-regulating sequences (TRSs) and create a junction with downstream sequence elements that code for the other viral proteins. Quantitative reverse transcriptase polymerase chain reaction (RT-qPCR) is the commonly used method for sensitive and specific detection method for SARS-CoV-2. In particular, targeting the vRNA derived from cell culture supernatants is suitable for the quantification of genome copy equivalents (Toptan et al., 2020) while the detection of specific intracellular sgRNAs is used to quantify active viral replication (Shin et al., 2020; Wolfel et al., 2020; Kohmer et al., 2021). However, high costs, excessive hands on time, and reagent shortages emerging during the pandemic disqualify RT-qPCR for high-throughput testing.

In vitro cell culture models that can realistically mimic the viral replication cycle to decipher the pathology of COVID-19 are limited.

Primary human airway epithelial cells highly express both receptors ACE2 and TMPRSS2 and are permissive for SARS-CoV-2. They show CPEs 96 h post infection (Hoffmann et al., 2020b; Takayama, 2020), but have limited lifespan and thus difficult to handle or expensively available from commercial sources. Currently, the common cell lines for SARS-CoV-2 research are Caco2, Calu-3, Vero E6, HEK293T, and Huh7. Vero E6 cells have been shown to be susceptible to SARS-CoV-2 (Ogando et al., 2020). By introducing additional gene copies of TMPRSS2 they have been rendered even superior to infection when compared to the parental cell line by 2-log (Matsuyama et al., 2020). However, a severe impairment to work with these cells and to draw conclusions about the interaction with the host is only possible to a very limited extent, since an essential component of the type I interferon signaling pathway is defective (Osada et al., 2014). Caco2 are highly susceptible to SARS-CoV-2 and commonly used in our lab, showing a clear CPE (Bojkova et al., 2020b; Hoehl et al., 2020; Shin et al., 2020; Toptan et al., 2020). However, working with these human colon adenocarcinoma derived cells is very struggling, since CaCo2 have suboptimal growth properties in cell culture and inefficient transfection and selection properties and, thus, are only suitable to a limited extent for automatic high throughput analysis. In addition, two human lung epithelial cell lines, A549 (alveolar epithelial cell line) and Calu-3 (bronchial epithelial cell line) are available. Calu-3 cells are susceptible to SARS-CoV-2 infection (Bestle et al., 2020; Bojkova et al., 2020a) with a comparable efficiency when compared to Caco2 cells (Stanifer et al., 2020). In contrast to Calu-3, A549 cells have superior culturing properties compared to Caco2 cells and were shown to efficiently produce IFNγ (Torvinen et al., 2007) indicating an intact interferon chemokine signaling pathway. However, parental A549 cells are poorly infectable with SARS-CoV-2 (Hoffmann et al., 2020b).

The aim of this work was to establish a human lung cell based system that would allow SARS-CoV-2 infection experiments in a cell model that is easy to maintain, suitable for large-scale propagation and automated readout, and importantly to express interferon stimulated genes (ISGs) upon treatment with Type I/III and II interferons. Furthermore, an inducible gene overexpression cassette, for the investigation of cellular host restriction or dependency factors should be implemented.
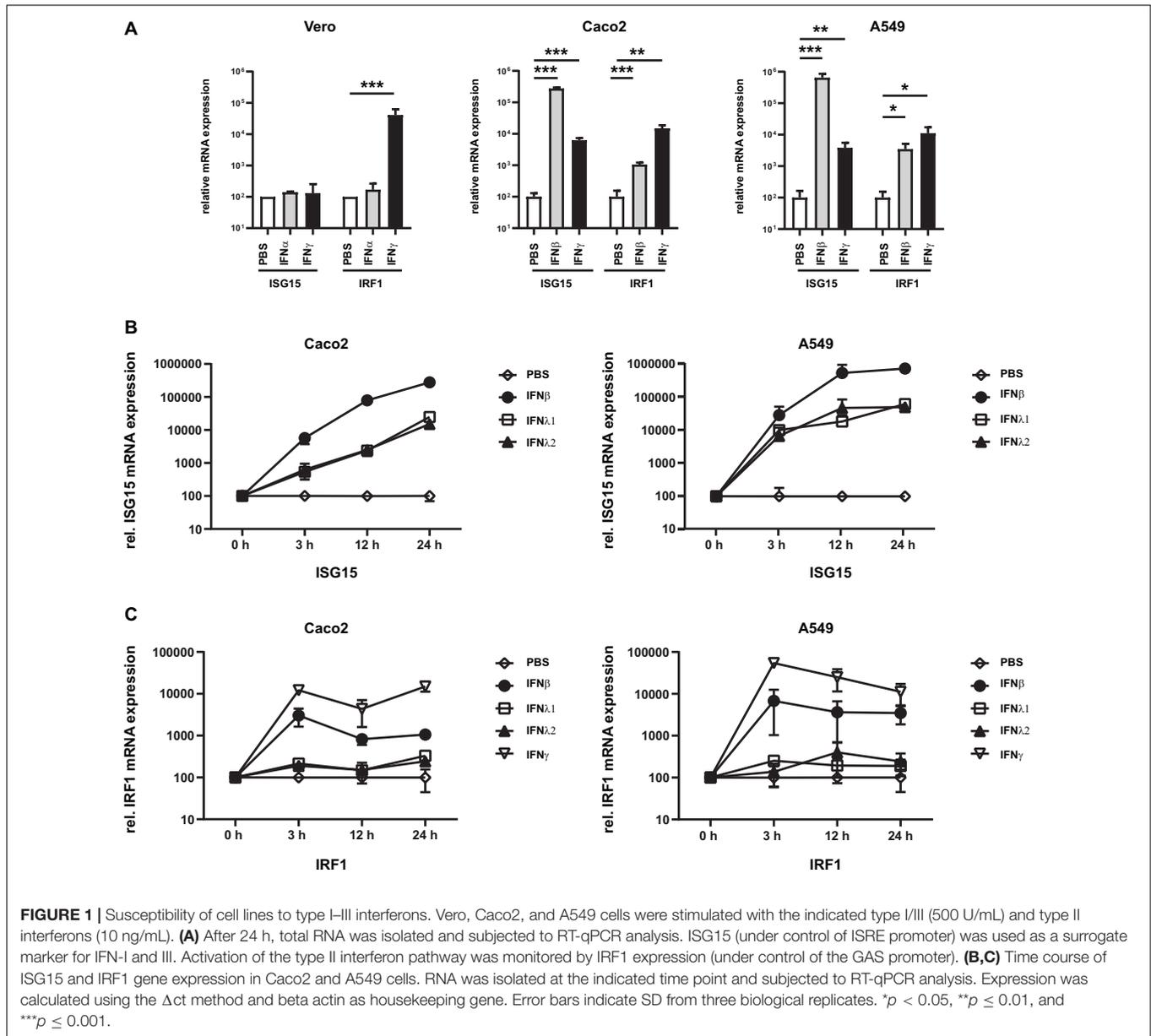
RESULTS

The major prerequisites for a novel model cell line for high throughput SARS-CoV-2 research are easy cultivation properties, reproducibility, relatively unlimited availability, but also pronounced interferon responses. As a suitable starting point, we have chosen the adenocarcinomic human alveolar basal epithelial cells A549 cells (Giard et al., 1973) and initially tested the susceptibility to interferons in comparison to in SARS-CoV-2 research commonly used Caco2 and Vero cells. Cells were stimulated with either type I or II interferons and the mRNA expression levels of known ISGs were examined by RT-qPCR. As surrogate markers for ISGs, we have chosen the two genes interferon-stimulated gene 15 (ISG15) and interferon regulatory factor 1 (IRF1), which are predominantly stimulated by type I/III or II interferons, respectively, and are significantly involved in host cell defense against SARS-CoV-2 (Shin et al., 2020; Karki et al., 2021). Compared to Caco2 cells (24-fold), an approximately 10-fold higher expression of ISG15 was detected in A549 cells (275-fold) when treated with type I interferon (**Figure 1A**). In Vero cells no ISG15 expression was observed after IFN-I stimulation confirming the defect in IFN-I signaling (Osada et al., 2014). In all cell lines IFN-γ treatment resulted in >2 log induction of IRF1 expression (345-fold in Caco2; 348-fold in A549 cells; and 412-fold IRF1 increase in Vero cells). A certain crosstalk could also be observed, since IFN-γ treatment of A549 and Caco2 cells resulted in a moderate but highly significant increase of ISG15 expression. Due to the defect in type I interferon signaling, Vero cells were excluded from further analysis.

Next, the time course of the ISG induction between A549 and Caco2 cells was investigated and two type III interferons (IFN-λ1 and -λ2), which have a distinct receptor to type I interferons but share common downstream signaling cascade, were also added. In both A549 and Caco2 cells, treatment with IFN-β (type I IFN) resulted in a strong increase with higher ISG15 expression levels, while both IFN-λ subtypes induced a similar increase and maximal level which were about 1 log level lower when compared with IFN-β treated cells (**Figure 1B**). IRF1 expression could be induced most strongly by IFN-γ while a moderate expression could be measured after IFN-β stimulation (**Figure 1C**). The maximum value was measured at 3 h after stimulation. Stimulation with IFN-lambda resulted in marginal ISG expression only. These data indicate that the A549 is suitable cell line to study type I, II, and III interferon dependent effects.

Since the choice of a cell line for high-throughput purposes depends largely on its properties in cell culture, we compared

proliferation rate, trypsinization and transfection efficiency of A549 and Caco2 cells. For this purpose, cells were seeded with low density and the cell growth was monitored over a period of 16 days using an automated confluence measurement and cell counting system. Exponential proliferation in A549 was observed immediately after seeding reaching full confluency at day 8 (**Figure 2A**). Caco2 cells proliferated in a biphasic manner, with very slow growth observed for the first few days (until about day 4), reaching a 50% confluency at day 8, and approximately 75% at day 15. A further characteristic for efficient use is the duration of trypsinization until full detachment of the cells prior to splitting for experiments. A549 cells required a significantly shorter time than Caco2 cells, which were detached from a plate after around 3 min (**Figure 2B**). Finally, the transfection efficiency of the two cell lines was compared. A green fluorescent protein (GFP)-encoding plasmid DNA (pSBtet GP) was used for transient transfection of both cell lines. Using standard conditions, we found that A549 cells allowed a 3.52-fold (24 h), and 1.81-fold (48 h) higher transfection efficiency than Caco2 cells (**Figures 2C,D**). These data confirmed that A549 have cell culture properties that are highly suitable for high-throughput analyses.
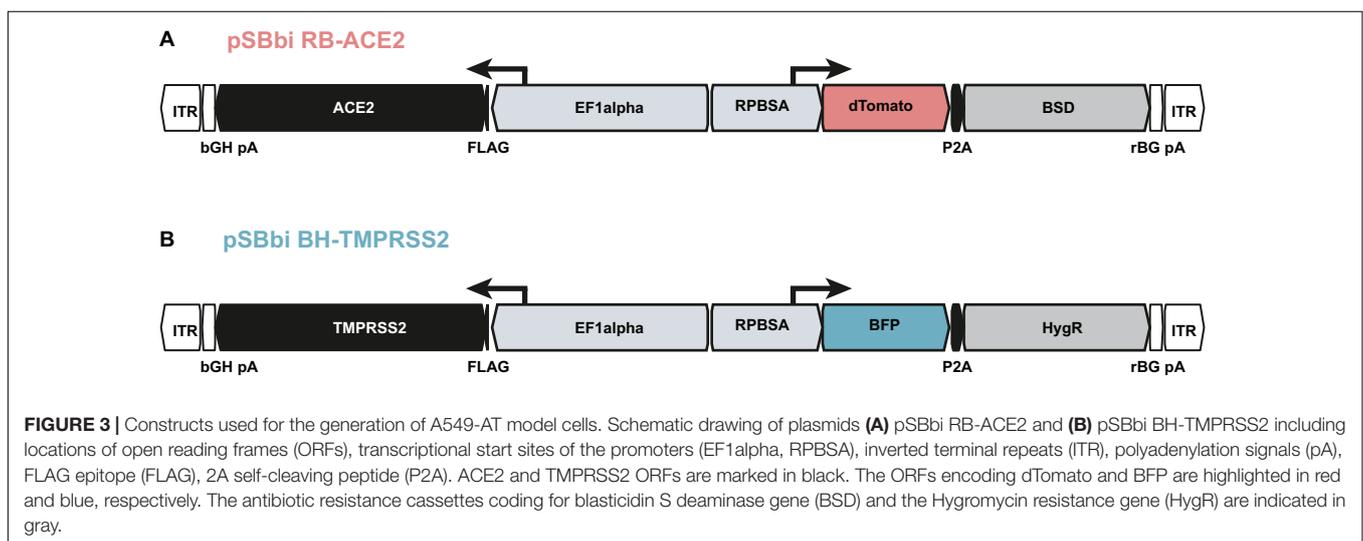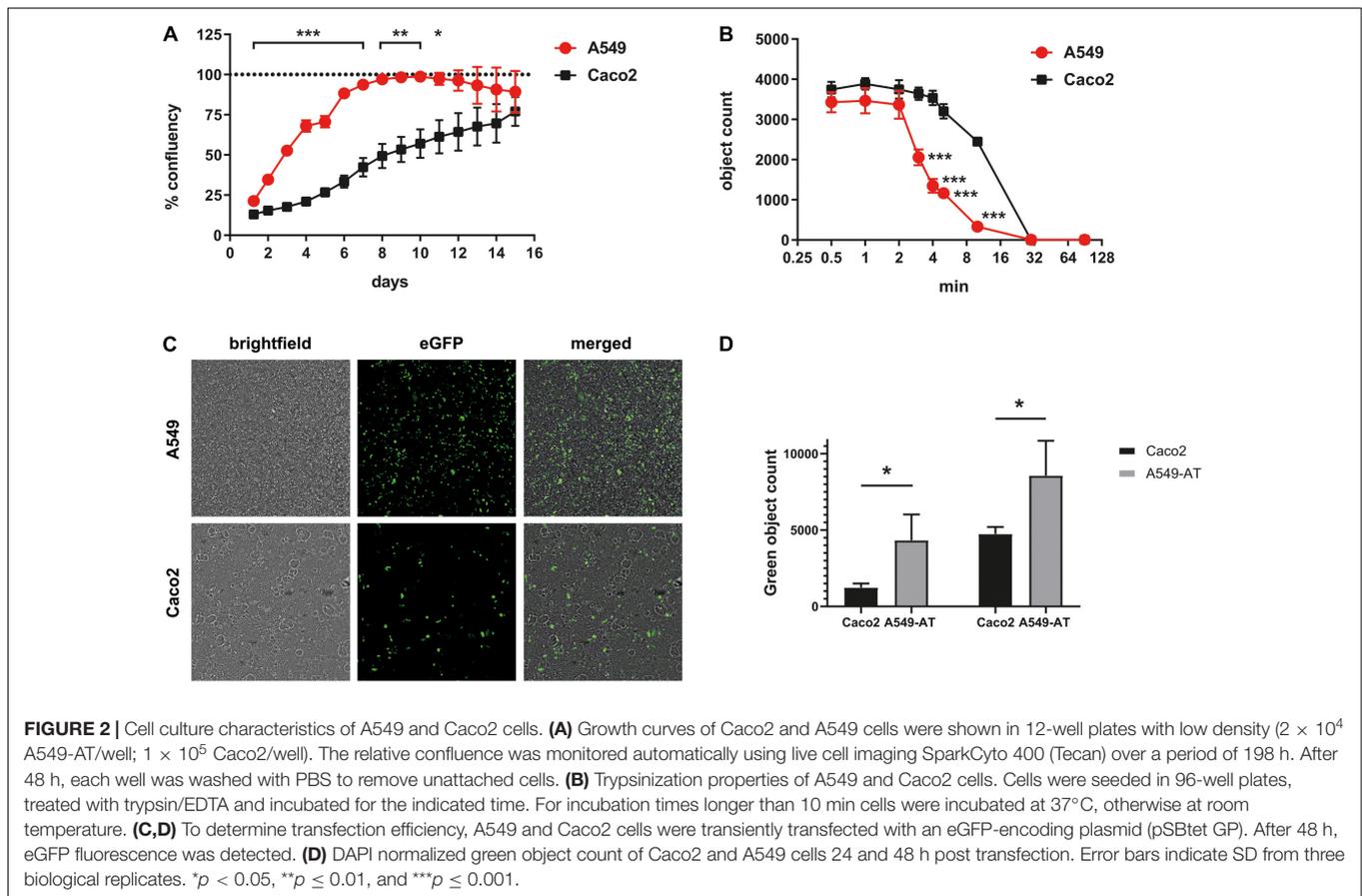
Since parental A549 cells are less susceptible to SARS-CoV and SARS-CoV-2 infection and *per se* do not allow CPE formation, we aimed to overexpress both the ACE2 receptor and TMPRSS2 protease (Hoffmann et al., 2020b) necessary for SARS-CoV-2 entry. We used the well-established Sleeping Beauty system (Kowarz et al., 2015), which enables transposase-mediated stable transfection of the target cells. For this purpose, we first generated a construct that allows constitutive expression of ACE2 together with an expression cassette for dTomato (**Figure 3A**) using blasticidin S deaminase (BSD) as a selection marker. A549 cells were transfected together with a transposase encoding plasmid to achieve *a priori* stable integration. Following antibiotic selection, we checked for ACE2 expression *via* western blotting and investigated the extent to which A549 cells can be infected in comparison to the highly susceptible Caco2. We infected parental and ACE2 expressing cell lines (named as low and high, based on the expression level) with SARS-CoV-2 isolate FFM1 and 24 h post infection the intracellular RNA and RNA from the cell culture supernatant was isolated and subjected to RT-qPCR (**Supplementary Figure 1**). Subgenomic SARS-CoV-2 RNA (sgRNA) was quantified as a marker of active virus replication, while the virus production of the infected cells was determined by detection of genome copy equivalents using the M gene. Compared to the Caco2 cells, A549 with high ACE2 expression cells could be infected more than 4 log more efficient with SARS-CoV and 2 log more efficient with SARS-CoV-2 (**Supplementary Figure 1**). However, in comparison to Caco2, 4 log lower infection efficiency was still observed. For constitutive expression of high levels of TMPRSS2, we used a similar construct with BFP and a hygromycin resistance gene cassette (HygR) with a constitutive TMPRSS2 expression under the control of the EF1alpha promoter (**Figure 3B**). Since both expression constructs carry different fluorescence cassettes (BFP and dTomato) under RPBSA promoter, we sorted cell populations with different expression levels of both proteins using flow

FIGURE 1 | Susceptibility of cell lines to type I–III interferons. Vero, Caco2, and A549 cells were stimulated with the indicated type I/III (500 U/mL) and type II interferons (10 ng/mL). **(A)** After 24 h, total RNA was isolated and subjected to RT-qPCR analysis. ISG15 (under control of ISRE promoter) was used as a surrogate marker for IFN-I and III. Activation of the type II interferon pathway was monitored by IRF1 expression (under control of the GAS promoter). **(B,C)** Time course of ISG15 and IRF1 gene expression in Caco2 and A549 cells. RNA was isolated at the indicated time point and subjected to RT-qPCR analysis. Expression was calculated using the Δct method and beta actin as housekeeping gene. Error bars indicate SD from three biological replicates. *$p < 0.05$, **$p \leq 0.01$, and ***$p \leq 0.001$.

cytometry and examined these cell lines for SARS-CoV-2 induced CPE formation. The population with the most distinct CPE was chosen, which, notably, was not the one with the highest expression intensity (Population 2, **Supplementary Figure 2**) and retrieved A549-ACE2^{high}-TMPRSS2^{low} cells (A549-AT).

To compare the properties of the A549-AT model cell line with respect to SARS-CoV-2 susceptibility with well-established Caco2 and parental A549 cells, all cell lines were infected with SARS-CoV-2 strain FFM1 (Toptan et al., 2020). A total of 24 h post infection cellular RNA was extracted and subjected to RT-qPCR detecting sgRNA as a surrogate marker specific for active viral replication. TMPRSS2 overexpression was not sufficient to render A549 cells susceptible to SARS-CoV-2 (**Figure 4A**). Although the expression of ACE2 resulted in a considerable increase in the amount of viral sgRNA, a further increase of 2 log levels
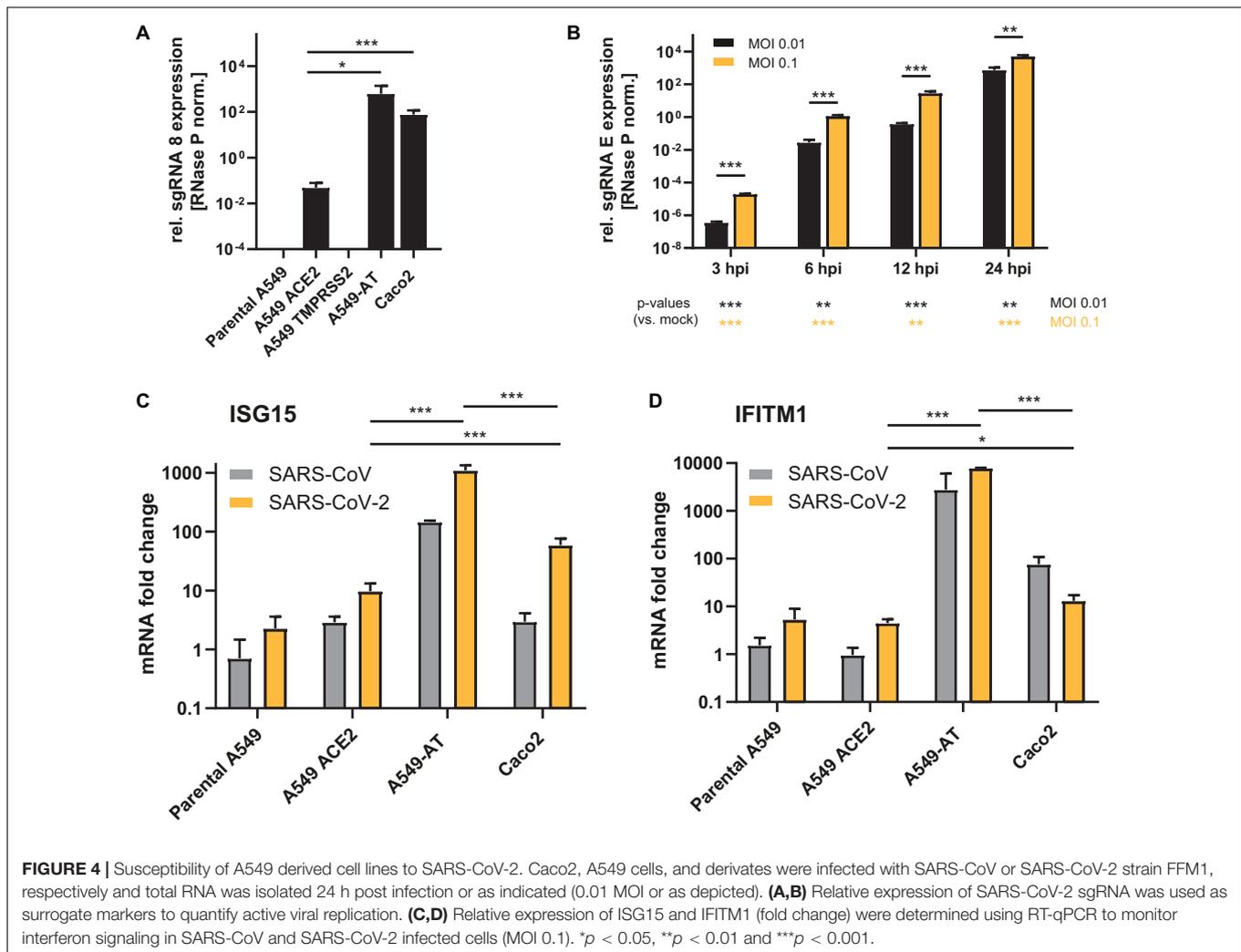
was achieved in combination with the additionally introduced TMPRSS2 (**Figure 4A**). This efficiency was thus comparable and even slightly higher when compared to Caco2 cells. Already 3 h after infection, sgRNA species could be detected, with a significant increase measured at 24 h after infection (**Figure 4B**). As expected, the addition of 10-fold more virus (MOI 0.1) resulted in a proportional increase in the sgRNA level. Consistent with **Figure 1**, a marked increase in ISGs (ISG15 and IFITM1) was observed in A549-AT with both SARS-CoV and SARS-CoV-2 (**Figures 4C,D**). The induction of both ISGs was 2 log higher for SARS-CoV and about 1 log higher for SARS-CoV-2 (ISG15) compared to Caco2 cells. IFITM1 expression was induced by 2 log after infection with SARS-CoV and even 3 log for SARS-CoV-2. Using RT-qPCR and cell based infection assays, we were able to demonstrate that the cell culture supernatant of infected

FIGURE 2 | Cell culture characteristics of A549 and Caco2 cells. **(A)** Growth curves of Caco2 and A549 cells were shown in 12-well plates with low density (2×10^4 A549-AT/well; 1×10^5 Caco2/well). The relative confluence was monitored automatically using live cell imaging SparkCyto 400 (Tecan) over a period of 198 h. After 48 h, each well was washed with PBS to remove unattached cells. **(B)** Trypsinization properties of A549 and Caco2 cells. Cells were seeded in 96-well plates, treated with trypsin/EDTA and incubated for the indicated time. For incubation times longer than 10 min cells were incubated at 37°C, otherwise at room temperature. **(C,D)** To determine transfection efficiency, A549 and Caco2 cells were transiently transfected with an eGFP-encoding plasmid (pSBtet GP). After 48 h, eGFP fluorescence was detected. **(D)** DAPI normalized green object count of Caco2 and A549 cells 24 and 48 h post transfection. Error bars indicate SD from three biological replicates. *$p < 0.05$, **$p \leq 0.01$, and ***$p \leq 0.001$.

FIGURE 3 | Constructs used for the generation of A549-AT model cells. Schematic drawing of plasmids **(A)** pSBbi RB-ACE2 and **(B)** pSBbi BH-TMPRSS2 including locations of open reading frames (ORFs), transcriptional start sites of the promoters (EF1alpha, RPBSA), inverted terminal repeats (ITR), polyadenylation signals (pA), FLAG epitope (FLAG), 2A self-cleaving peptide (P2A). ACE2 and TMPRSS2 ORFs are marked in black. The ORFs encoding dTomato and BFP are highlighted in red and blue, respectively. The antibiotic resistance cassettes coding for blasticidin S deaminase gene (BSD) and the Hygromycin resistance gene (HygR) are indicated in gray.

A549-AT cells contained replication-competent virus, indicating productive infection of A549-AT cells (**Supplementary Figure 3**). Taken together, the data show that the newly generated model cell line allows robust, time- and concentration-dependent viral replication and induction of strong innate response.

To monitor SARS-CoV-2 replication non-invasively, we used an automated cell imaging system (SparkCyto 400, Tecan). First, we infected the cells with SARS-CoV-2 strain FFM1 (Toptan et al., 2020) and examined the cells for CPE formation. In comparison to the Caco2 cells, we could already observe CPE formation and loss of confluency after 12 h post infection (**Figure 5A**). In addition, an increasing roughness of the cells could be observed (**Figure 5B**) due to the formation of syncytia and cell lysis (**Figures 5C,D** and **Supplementary Movie 1**).

FIGURE 4 | Susceptibility of A549 derived cell lines to SARS-CoV-2. Caco2, A549 cells, and derivates were infected with SARS-CoV or SARS-CoV-2 strain FFM1, respectively and total RNA was isolated 24 h post infection or as indicated (0.01 MOI or as depicted). **(A,B)** Relative expression of SARS-CoV-2 sgRNA was used as surrogate markers to quantify active viral replication. **(C,D)** Relative expression of ISG15 and IFITM1 (fold change) were determined using RT-qPCR to monitor interferon signaling in SARS-CoV and SARS-CoV-2 infected cells (MOI 0.1). $*p < 0.05$, $**p < 0.01$ and $***p < 0.001$.

This effect was clearly distinguishable from the non-infected cells (>100-fold) and was proportional to the cell lysis and the associated loss of confluence. Thus, cellular roughness represents an excellent marker for estimating the CPE, which appears prior to confluence changes. Caco2 cells also showed a clear reduction in confluency and an altered roughness, which however could only be read out automatically to a limited extent in comparison to A549-AT (**Figure 5** and **Supplementary Movies 2, 3**). The effects were clearly evident at an intermediate MOI of 1, while lower MOIs (0.1 and 0.01) led to a time-delayed onset of roughness and confluency loss. A549-AT were also suitable to display the CPE of various SARS-CoV-2 isolates including variants of concern (VoCs) B.1.1.7 (including Spike N501Y) and P.2 (including Spike E484K), which have been associated with higher transmission and immune escape, respectively (Widera et al., 2021b; **Figures 5D–F**).

Quantifying the loss of dTomato signal upon viral infection constitutes a third read-out assay to monitor CPE formation. This is particularly suitable for fluorescence based measurement, which is a time and resource efficient readout method. The optimal time to monitor fluorescence in SARS-CoV-2 infected cells was at 48 h post-inoculation for complete CPE (MOI 0.01 and 0.1) (**Figures 5G,H**), and less than 24 h post-inoculation for early CPE (MOI 0.1 and 1) (see below). These data demonstrate that the A549-AT model cell line is suitable for numerous automated readout methods and for determining SARS-CoV-2 replication.

Next, we evaluated to which extent the A549-AT model cell line is suitable for drug screenings, testing antiviral drugs and monoclonal neutralizing antibodies (mAbs). For this purpose, we pre-treated cells with increasing amounts of the well described antiviral compound remdesivir and infected the cells with SARS-CoV-2 strain FFM1 (**Figures 6A,B**). In agreement with current literature (Wang M. et al., 2020), we estimated an IC50 of 47.95 nM using relative confluency and roughness. To verify the functionality of TMPRSS2, we additionally treated infected cells with camostat (**Figures 6C–F**). A significant reduction in virus replication was observed at an EC50 concentration of 137 nM, which was in line with previously published data reporting an IC50 of 107 nM (Hoffmann et al., 2021b). Noteworthy, we were also able to reproduce our results conducting fluorescence intensity measurements, which
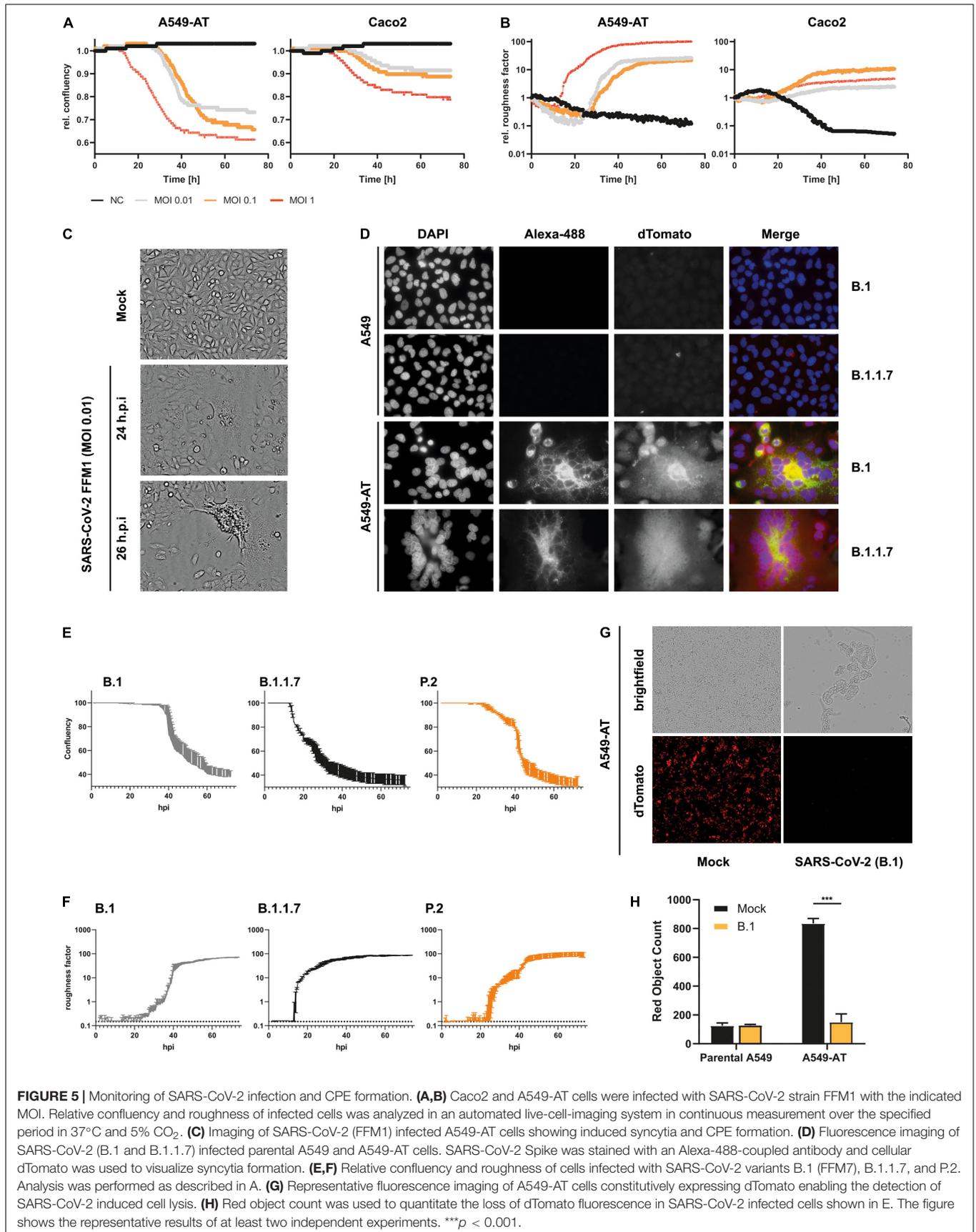
FIGURE 5 | Monitoring of SARS-CoV-2 infection and CPE formation. **(A,B)** Caco2 and A549-AT cells were infected with SARS-CoV-2 strain FFM1 with the indicated MOI. Relative confluency and roughness of infected cells was analyzed in an automated live-cell-imaging system in continuous measurement over the specified period in 37°C and 5% CO_2. **(C)** Imaging of SARS-CoV-2 (FFM1) infected A549-AT cells showing induced syncytia and CPE formation. **(D)** Fluorescence imaging of SARS-CoV-2 (B.1 and B.1.1.7) infected parental A549 and A549-AT cells. SARS-CoV-2 Spike was stained with an Alexa-488-coupled antibody and cellular dTomato was used to visualize syncytia formation. **(E,F)** Relative confluency and roughness of cells infected with SARS-CoV-2 variants B.1 (FFM7), B.1.1.7, and P.2. Analysis was performed as described in A. **(G)** Representative fluorescence imaging of A549-AT cells constitutively expressing dTomato enabling the detection of SARS-CoV-2 induced cell lysis. **(H)** Red object count was used to quantitate the loss of dTomato fluorescence in SARS-CoV-2 infected cells shown in E. The figure shows the representative results of at least two independent experiments. ***$p < 0.001$.
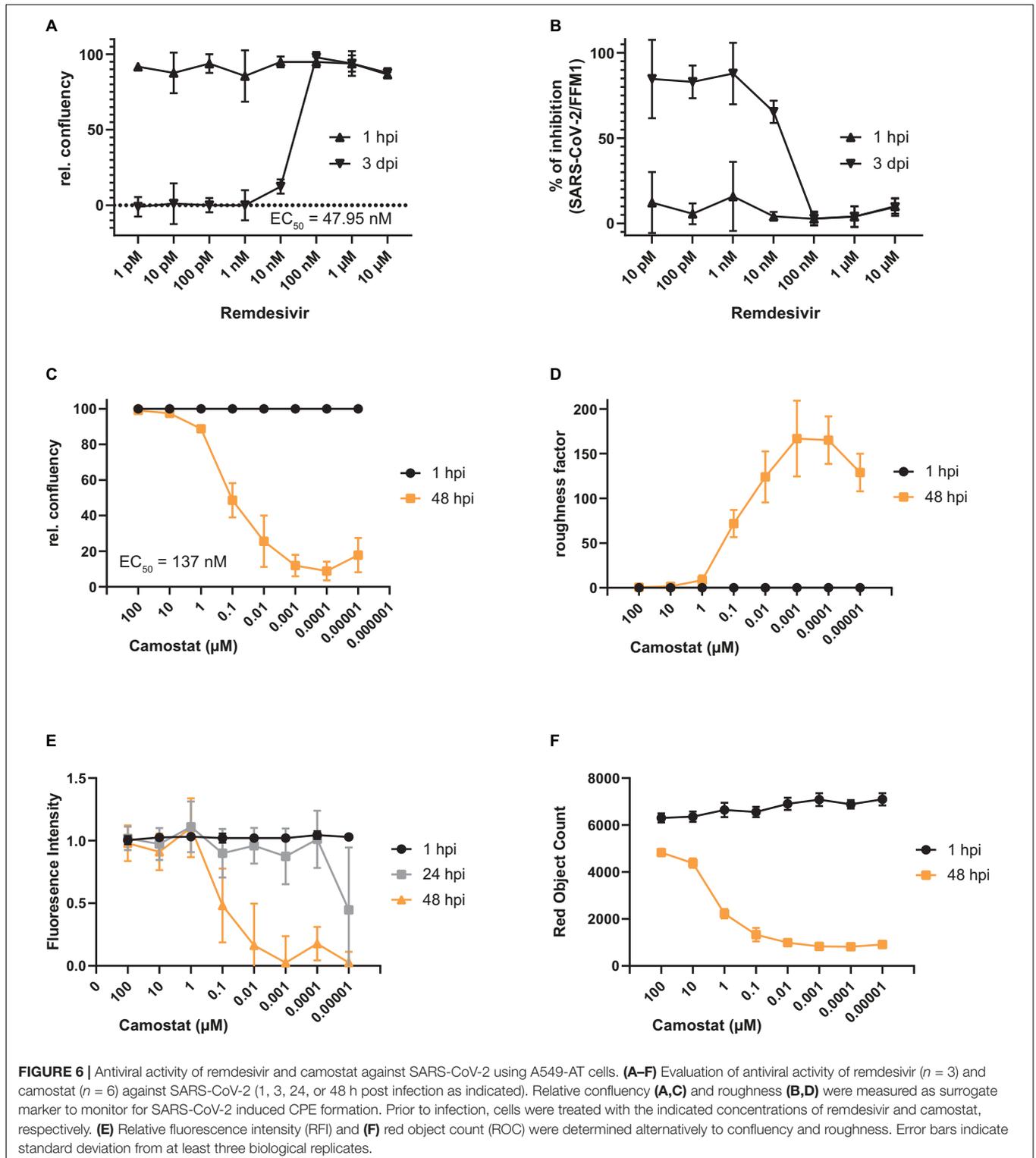
FIGURE 6 | Antiviral activity of remdesivir and camostat against SARS-CoV-2 using A549-AT cells. **(A–F)** Evaluation of antiviral activity of remdesivir ($n = 3$) and camostat ($n = 6$) against SARS-CoV-2 (1, 3, 24, or 48 h post infection as indicated). Relative confluency **(A,C)** and roughness **(B,D)** were measured as surrogate marker to monitor for SARS-CoV-2 induced CPE formation. Prior to infection, cells were treated with the indicated concentrations of remdesivir and camostat, respectively. **(E)** Relative fluorescence intensity (RFI) and **(F)** red object count (ROC) were determined alternatively to confluency and roughness. Error bars indicate standard deviation from at least three biological replicates.

represents an additional time- and resource efficient readout method (**Figure 6E**).

Next, we determined $TCID_{50}$ titers of various SARS-CoV-2 isolates and compared the values of A549-AT with Caco2 derived

$TCID_{50}$ titers, which were well correlating (**Figure 7A**). Since mAbs and neutralizing titers of patient derives sera are important factors in SARS-CoV-2 immunity, we used A549-AT cells and determined neutralization ab titers. The reciprocal antibody titers
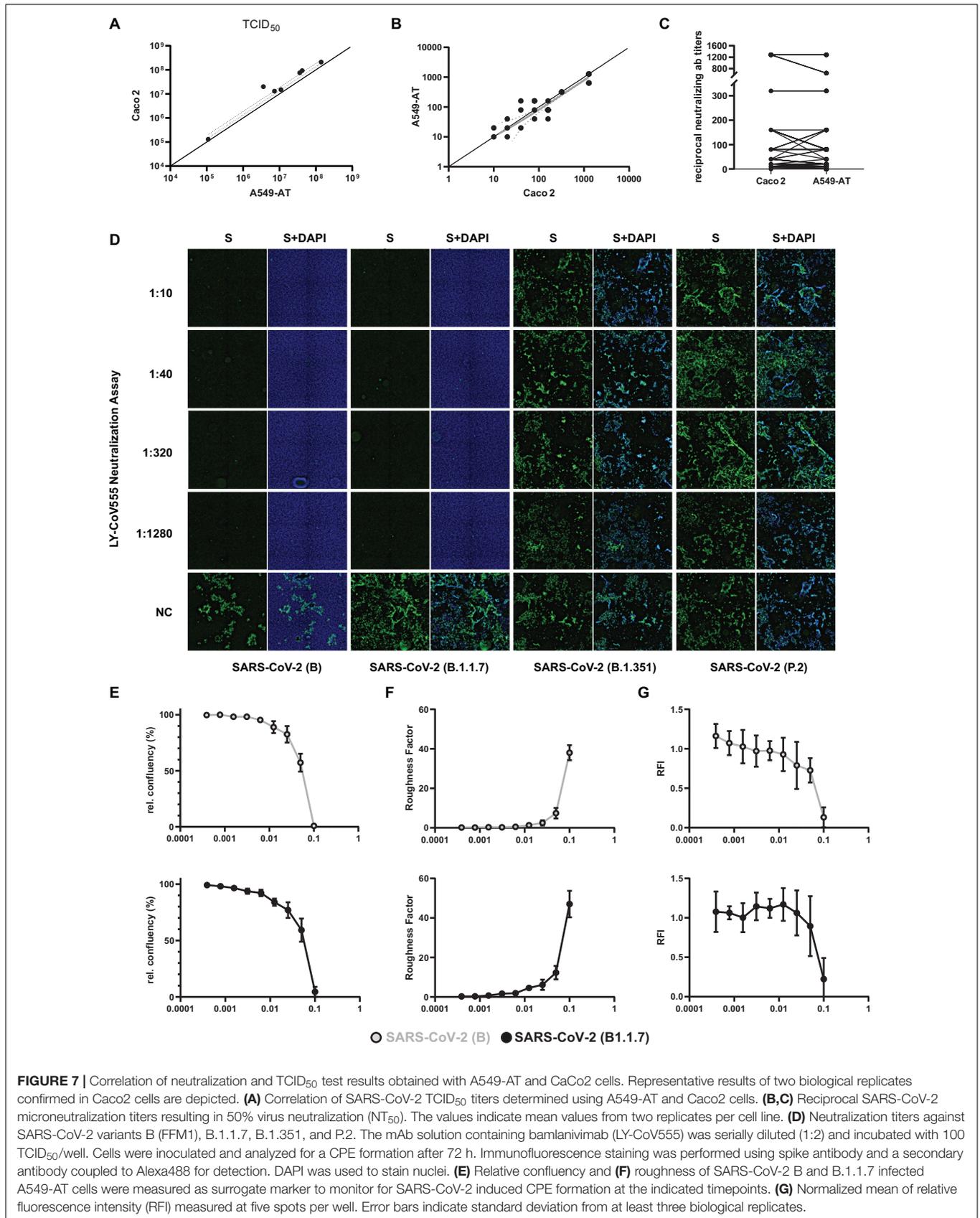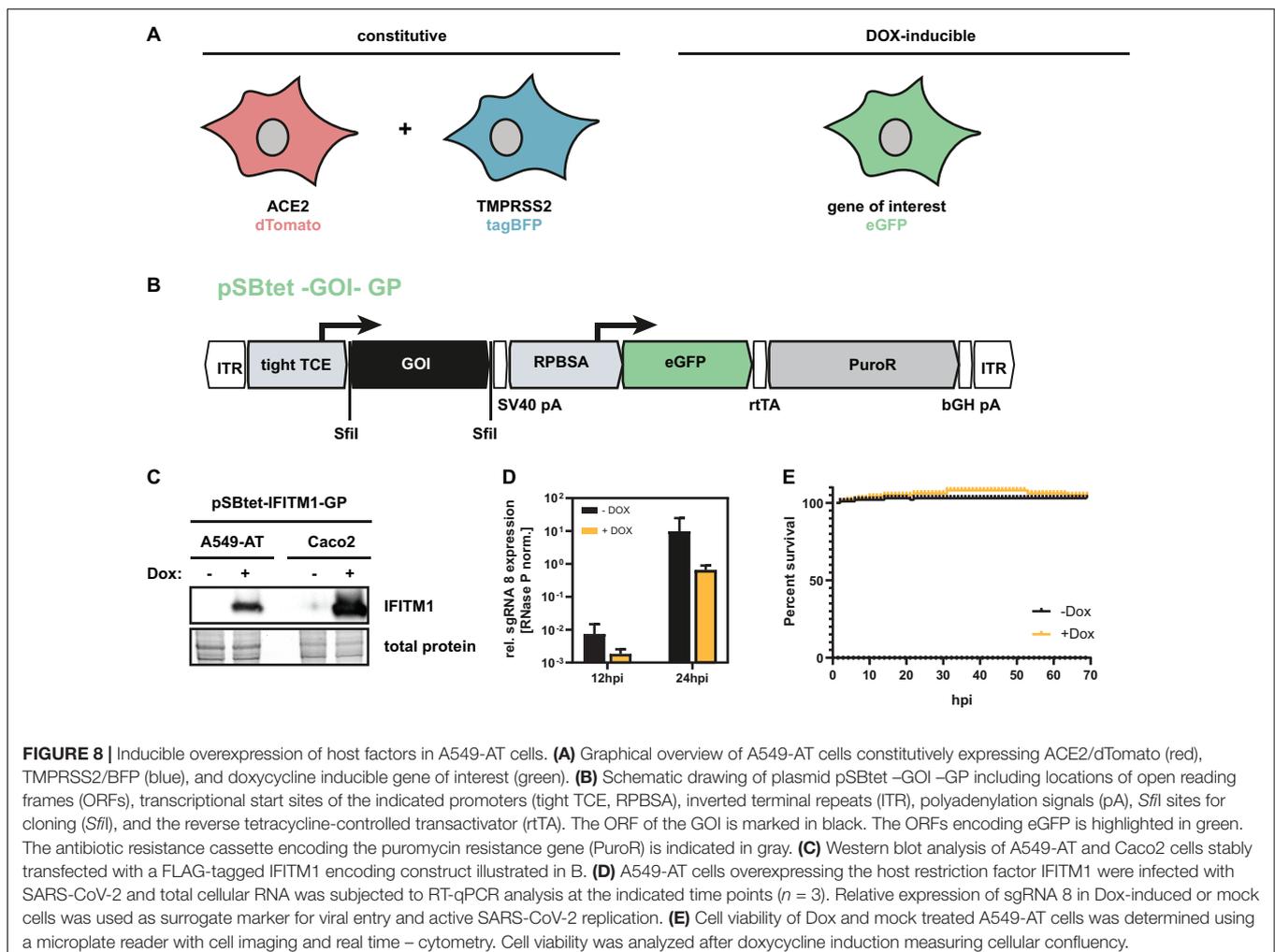
FIGURE 7 | Correlation of neutralization and TCID$_{50}$ test results obtained with A549-AT and CaCo2 cells. Representative results of two biological replicates confirmed in Caco2 cells are depicted. (A) Correlation of SARS-CoV-2 TCID$_{50}$ titers determined using A549-AT and Caco2 cells. (B,C) Reciprocal SARS-CoV-2 microneutralization titers resulting in 50% virus neutralization (NT$_{50}$). The values indicate mean values from two replicates per cell line. (D) Neutralization titers against SARS-CoV-2 variants B (FFM1), B.1.1.7, B.1.351, and P.2. The mAb solution containing bamlanivimab (LY-CoV555) was serially diluted (1:2) and incubated with 100 TCID$_{50}$/well. Cells were inoculated and analyzed for a CPE formation after 72 h. Immunofluorescence staining was performed using spike antibody and a secondary antibody coupled to Alexa488 for detection. DAPI was used to stain nuclei. (E) Relative confluency and (F) roughness of SARS-CoV-2 B and B.1.1.7 infected A549-AT cells were measured as surrogate marker to monitor for SARS-CoV-2 induced CPE formation at the indicated timepoints. (G) Normalized mean of relative fluorescence intensity (RFI) measured at five spots per well. Error bars indicate standard deviation from at least three biological replicates.

were determined with A549-AT and had an excellent correlation to titers obtained with Caco2 cells (**Figures 7B,C**). SARS-CoV-2 neutralization titer assays showing limiting neutralizing capacity of commercial mAb bamlanivimab (LY-CoV555) against E484K carrying SARS-CoV-2 isolates (Widera et al., 2021b) was also confirmed using immunofluorescence staining. SARS-CoV-2 variant B.1.1.7, as well as the isolates from early 2020 (FFM1 and FFM7), could be efficiently neutralized by LY-CoV555 (titer 1/1280), respectively (**Figure 7D**). However, no neutralization effect could be observed against either B.1.351 or P.2, both harboring the E484K substitution. By measuring the relative cell confluence (**Figure 7E**) and roughness (**Figure 7F**), we were able to monitor a concentration-dependent effect of the neutralizing antibody on CPE formation of SARS-CoV-2 B and B.1.1.7 infected A549-AT cells with an EC_{50} of 0.054 and 0.055 µg/ml, respectively. Due to the constitutive dTomato expression, we were also able to detect the infection induced cell lysis by rapid fluorescence measurement (**Figure 7G**). The relative fluorescence intensity (RFI) was comparable to the image-based evaluation method, however, due to the limited amount of measuring points (five per well), the values had a

higher deviation. These data highlights that our A549-AT cells are suitable for high-throughput screening for antiviral compounds as well as for investigating the efficacy of neutralizing antibodies against different SARS-CoV-2 variants.

Since A549-AT was found suitable for automated readout of SARS-CoV-2 infection experiments, viral outgrowth assays as well as drug screenings and neutralization tests, we next focused on the investigation of cellular restrictions and dependency factors. For this purpose, we generated a third vector based on the Sleeping Beauty transposase system, which has a doxycycline (Dox) inducible expression cassette (**Figures 8A,B**). In addition to the gene of interest, which is expressed under the inducible TCE promoter, the constructs also contain a cassette encoding the GFP and an additional resistance cassette (PuroR) for antibiotic selection. To provide a proof of principle, we cloned the known host restriction factor IFITM1, which has an antiviral effect against SARS-CoV-2, into the expression cassette. A549 and for comparison purposes Caco2 cells were stably transfected with these constructs and subjected to antibiotic selection. As validated with Western blotting, 48 h after doxycycline addition, maximum overexpression of IFITM1 could be achieved

FIGURE 8 | Inducible overexpression of host factors in A549-AT cells. **(A)** Graphical overview of A549-AT cells constitutively expressing ACE2/dTomato (red), TMPRSS2/BFP (blue), and doxycycline inducible gene of interest (green). **(B)** Schematic drawing of plasmid pSBtet –GOI –GP including locations of open reading frames (ORFs), transcriptional start sites of the indicated promoters (tight TCE, RPBSA), inverted terminal repeats (ITR), polyadenylation signals (pA), *Sfi*I sites for cloning (*Sfi*I), and the reverse tetracycline-controlled transactivator (rtTA). The ORF of the GOI is marked in black. The ORFs encoding eGFP is highlighted in green. The antibiotic resistance cassette encoding the puromycin resistance gene (PuroR) is indicated in gray. **(C)** Western blot analysis of A549-AT and Caco2 cells stably transfected with a FLAG-tagged IFITM1 encoding construct illustrated in B. **(D)** A549-AT cells overexpressing the host restriction factor IFITM1 were infected with SARS-CoV-2 and total cellular RNA was subjected to RT-qPCR analysis at the indicated time points (*n* = 3). Relative expression of sgRNA 8 in Dox-induced or mock cells was used as surrogate marker for viral entry and active SARS-CoV-2 replication. **(E)** Cell viability of Dox and mock treated A549-AT cells was determined using a microplate reader with cell imaging and real time – cytometry. Cell viability was analyzed after doxycycline induction measuring cellular confluency.

(**Figure 8C**). Addition of doxycycline prior to infection resulted in a marked decrease in SARS-CoV-2 sgRNA levels, indicating inhibited virus entry (**Figure 8D**). Of note, the addition of doxycycline itself had no effect on cell viability (**Figure 8E**).

In summary, by using the Sleeping Beauty transposase system, we generated a robust and versatile model cell line that allows SARS-CoV-2 infection experiments compatible for high-throughput and live cell imaging. Sleeping Beauty transposase-based overexpression and shRNA based knockdown cell lines with a second constitutive fluorescence reporter cassette (eGFP) can be generated in a very short time, enabling the investigation of host and restriction factors in a doxycycline -inducible manner.

DISCUSSION

Severe acute respiratory syndrome coronavirus 2 research studies require appropriate cell culture model systems. However, the current methods to monitor and quantitate SARS-CoV-2 infectivity in cell culture are time-consuming and labor-intensive. The A549-AT system established in this work allows to study the interactions between SARS-CoV-2 and the host cell in a high throughput setup at low cost. In addition, assays common in antiviral research can be transferred to an A549-AT setting with comparable results, but in less time.

The cell line A549 was established in 1972 by Giard et al. (1973) by culturing an explant of lung carcinoma tissue from a 58-year-old male Caucasian patient. The alveolar adenocarcinoma cell line (alveolar type II-like) combines a lung-associated background with the advantages of an easy-to-handle cell system. In our study, we compared the properties of the A549 cell line to Caco2 well established in the field and in our lab (Bojkova et al., 2020b; Shin et al., 2020; Toptan et al., 2020) and found clear advantages in terms of proliferation, trypsinization, and transfection efficiency (**Figure 2**). In addition, A549 cells can be subjected to efficient antibiotic selection, as significantly lower concentrations and treatment times are required when compared to Caco2 cells (data not shown). Another advantage become apparent during microscopic observation, as Caco2 cells are a very heterogeneous cell line (Lea, 2015), while A549 have a much more homogeneous morphology (**Figure 2**).

Cellular entry of coronaviruses is a multistage process involving virus attachment to the cell surface, receptor engagement, protease processing and membrane fusion (Li et al., 2021). These stages rely on distinct domains in the SARS-CoV-2 spike protein (Lan et al., 2020). Emerging SARS-CoV-2 VOCs like B.1.1.7, B.1.351, P.1, and B.1.617.2 initially observed in the United Kingdom, South Africa, Brazil, and India, respectively, harbor amino acid substitutions in the receptor binding domain of the Spike protein (Garcia-Beltran et al., 2021; Hoffmann et al., 2021a). First and foremost, N501Y was described to increased infectivity due to enhanced receptor binding (Starr et al., 2020). Further studies have shown that E484 represents an immunodominant site on the RBD since E484K reduced naturalization capacity of human convalescent sera by >100-fold (Greaney et al., 2021; Widera et al., 2021b). These amino acid substitutions have also been observed to

evade the antibody response elicited by an infection with other SARS-CoV-2 variants, or vaccination. In this work we could show that A549-AT cells were susceptible to multiple variants allowing studies with a broad range of viral strains. In addition, mutagenesis of ACE2 or TMPRSS2 and subsequent phenotypical characterization can be performed with our system.

Through the stable integration of fluorescent proteins, in particular the constitutive dTomato expressing cassette localized on the ACE2 expression vector (**Figure 3**), the model cell line enables fast and automatic readout using red fluorescence for CPE and confluency determination. By using the additional Dox-inducible system (pSBTet-GP vector backbone), also cellular host factor can be overexpressed in order to study and dissect SARS-CoV-2 biology. All successful transfection experiments can be easily monitored by the expressed color tags which also allow the automation of all subsequent screening experiments.

In addition to the loss in fluorescence, two non-invasive factors can also be used as surrogate markers for CPE formation and cell lysis, which are confluency and roughness. The former was proofed as highly robust and was additionally confirmed with DAPI staining (data not shown). Exclusively in A549-AT, cellular roughness was used to monitor syncytia formation which was much less pronounced in Caco2 cells. Furthermore, a clear CPE formation could be monitored since A549 have a less heterogenic morphology than Caco2 (**Figure 5**).

VeroE6 cells or VeroE6/TMPRSS2 cells, which are kidney epithelial cells extracted from an African green monkey, are also commonly used cells for SARS-CoV-2 studies. For certain applications such as the screening for potential host dependency or interferon induced restriction factors, it might be important to have an infection model akin to a human lung. A further advantage over Vero/TMPRSS2 cells, which also show CPE formation with detachment/floating and syncytium formation, is the red-fluorescent expression cassette offering a very fast automated plate-readout and quantification of the CPE. An important factor to study virus-host cell interactions is the ability to physiological respond to external stimuli and to induce a physiological antiviral response. Thus, we tested the interferon signaling pathways by treatment with interferon types I, II, and III (IFNs I–III). The IFN-I signaling deficiency in Vero cells allows several viruses to replicate efficiently. However, to study physiological responses to viral infections, intact interferon signaling is mandatory. In our study and in line with other studies (Li et al., 2021), we observed the induction of the type I interferon-induced genes ISG15 and IFITM1 correlating with the efficiency of virus entry (**Figure 3**). Consistently, insertion of an ACE2 expression cassette to parental A549 cells led to a small increase in ISG15 expression after SARS-CoV-2 infection, which was significantly increased by additional insertion of TMPRSS2. This increase correlated with the amount of detected sgRNA, which is a surrogate marker of active viral replication (Kim et al., 2020; Wolfel et al., 2020), and was higher in A549 cells when compared to SARS-CoV-2 infected Caco2 cells. Noteworthy, in both cell lines we observed higher ISG15 levels after SARS-CoV-2 infection compared to SARS-CoV infection, which was in line with previously published data showing a higher interferon antagonizing capacity of SARS-CoV (Shin et al., 2020).

In humans, type I interferons consist of IFN-α, β (ε, κ, and ω), while especially IFN-α consists of multiple subtypes with distinct biological activities (Lavender et al., 2016). While type I interferons are mostly produced by infected cells and cells of the immune system, type II interferon (IFN-γ) is predominantly produced by immune cells. In our study IRF1 expression was used as a surrogate marker of IFN-II induction and was induced in Vero, Caco2 and A549 cells to a comparable extent. Importantly, IFN-γ driven inflammation was shown to induce a vulnerable state *in vivo* allowing SARS-CoV-2 replication by promoting ACE2-expression and enhanced virus production in infected cells (Heuberger et al., 2021). Hence, A549-AT cells are suitable to study cell culture based responses to IFN-γ.

Type III interferons consist of four subtypes of IFN-λ. Although some immune cells produce type III interferons, these are also produced by epithelial cells or cells that are from the same developmental stage, which are the respiratory tract, the gastrointestinal tract, and the urogenital tract derived cells. Type III IFNs were effective in preventing SARS-CoV-2 infection but are in contrast to IFN-I locally limited in the respiratory tract (Andreakos and Tsiodras, 2020), which makes them relevant for treatment in early infected patients. Hence, it will be also interesting to analyze the impact of type III interferons on different SARS-CoV-2 variants in future.

Although lentiviral transduction is relatively quick, the compatibility of a gene of interest, which has to be cloned into a sophisticated vector, is size restricted and does not allow polyA and splicing sites, which might interfere with the LTR-mediated integration of the transgene into the host chromosome. Random integration into genome preferentially in transcriptionally active regions might cause cell cycle defects. Depending on several factors a varying copy number of integrations might occur. Furthermore, the preparation of lentiviruses requires biosafety level 2 (BSL-2) lab work. In contrast, transposable elements as the Sleeping Beauty (Kowarz et al., 2015) offers several advantages for transgene integration. The use of *Sfi*I with distinct recognition sequences at the 5′ and 3′ site allows directional cloning with only one enzyme, which is rarely found in GOIs due to the long recognition sequence. In comparison to other methods Sleeping Beauty transposase is quick and might be performed under BSL-1 safety labs. Outstanding features are no size restriction, compatibility with the integration of polyA and splicing sites in the gene of interest region. Integration into genome occurs preferentially at TA-sites, however a certain limitation remains since a targeted integration at a predetermined location in the genome is not possible. Through precise dosing of the vector and the transposase-encoding plasmid scalable number of integrations can be achieved (Skipper et al., 2013).

A further conceivable development of the system would be a construct expressing eGFP enabling the parallel expression of an inducible shRNA-mediated knock-down cassette. This would allow loss-of-function experiments to be carried out in addition to gain-of-function experiments.

In conclusion, we developed a cellular infection model system with optimal ACE2/TMPRSS2 ratio for high SARS-CoV-2 susceptibility, syncytia and CPE formation. The confluency and particularly roughness of A549-AT cells represent a highly sensitive marker for early syncytia formation and CPEs. Thus, A549-AT cells allow the infection and readout of an experiment on the same working day. Using MOI of 1 the system theoretically allows infection and read-out within one working day performed *via* non-invasive roughness factor analysis.

MATERIALS AND METHODS

Cell Culture and Virus Propagation

Vero, A549 (and derivates), and Caco2 cells were cultured in Minimum Essential Medium (MEM) supplemented with 10% fetal calf serum (FCS), 4 mM L-glutamine, 100 IU/ml of penicillin, and 100 μg/ml of streptomycin at 37°C and 5% CO_2.

Cell free virus aliquots of SARS-CoV isolate FFM1 (Drosten et al., 2003) and SARS-CoV-2 isolates FFM1, FFM7, B.1.1.7, B1.351, and P.2 (Hoehl et al., 2020; Toptan et al., 2020; Widera et al., 2021a,b) were stored at −80°C and titers were determined by $TCID_{50}$ in Caco2 cells. GeneBank accession numbers of the SARS-CoV-2 strains: MT358638 (FFM1), MT358643 (FFM7), MW822592 (B.1.351), MW822593 (P.2), and MW822594 (B.1.1.7). According to the Committee on Biological Agents (ABAS) and Central Committee for Biological Safety (ZKBS) all infectious work was performed under BSL-3 conditions. Efficiency of virus inactivation were confirmed as previously described (Westhaus et al., 2020).

Interferon Stimulation

Vero, Caco2, and A549 cells were stimulated with the type I–III interferons (500 U/mL and 10 ng/mL, respectively. Total RNA was isolated and subjected to RT-qPCR analysis at the indicated time points.

Plasmids Construction and Cloning

Total RNA (1 μg) was isolated from HEK293T cells and reverse transcribed into cDNA using random hexamers and SuperScript II RT (Invitrogen). The ACE2 and TMPRSS2 genes were amplified with GoTaq polymerase (Promega) by using the oligonucleotides ACE2.Flag.Sfi.F, ACE2.Sfi.R, TMPRSS2.Flag.Sfi.F, and TMPRSS2.Sfi.R, respectively (**Supplementary Table 1**). All 3′-primers encode an additional N-terminal FLAG-tag as well as the 5′-*Sfi*I-restriction site, while the 5′-primers encode the additional 3′-*Sfi*I-restriction site. All amplimers were cloned into the PCR2.1-Topo-TA vector (Invitrogen) for Sanger sequencing. Correct amplimers were digested with Sfi1 and cloned into the pSBbi-RB (ACE2) or pSBbi-BH (TMPRSS2) Sleeping Beauty plasmids (Kowarz et al., 2015).

Generation of Stable Cell Lines

Using TransIT LT1 (Mirus) A549 and Caco2 cells were transfected with a transposase-encoding plasmid (SB100x) and the respective Sleeping Beauty construct (see above). A total of 48 h later, appropriate selection was carried out with hygromycin, puromycin, or blasticidin. A total of three rounds of selection were performed, each with a recovery phase lasting two doublings per cell line. Transfection efficiency was monitored by fluorescence microscopy using the fluorescent proteins dTomato

and mTag-BFP. A549-AT cells can be obtained from the authors on request.

Quantitative Proliferation and Trypsinization Assay

CaCo2 and A549-based cells were seeded in 12-well plates (2×10^4 A549-AT and 1×10^5 Caco2/well, respectively). Cells were incubated for 16 days at 37°C and 5% CO_2 and cell count and confluency was optically determined using SparkCyto 400 (Tecan) at regular intervals starting after 48 h after seeding. To allow attachment, cells were incubated for 48 h before monitoring. Prior to imaging the wells were washed using PBS and refilled with 2 ml culture medium. Trypsinization assay was performed in 96 well plates. After rinsing twice with PBS, confluent cells were treated with 100 µl trypsin (2 mg/ml) and incubated for different intervals. Cells were incubated at room temperature and 37°C for incubation times longer than 10 min. Subsequently cells were rinsed with cell culture medium, remaining cells were fixed with 3% PFA, and nuclei were stained with DAPI and analyzed with a plate reader (SparkCyto 400).

Automatic Monitoring of SARS-CoV-2 Infection and CPE Formation

Cell confluency measurements were performed using Spark Cyto 400 multimode reader with cell imager and environmental control module (Tecan) and SparkControl Software (Tecan). Relative cell confluence was calculated by normalizing the complete virus induced cell lysis to 0%. The dimensionless roughness factor calculated by the normalized mean standard deviation of pixel intensities over all separated areas provides a measuring tool for virus induced CPE within a well. Automatic monitoring was performed at least with multiple biological replicates and confirmed by bright-field microscopy. The standard deviation within the replicates was indicated by the error bars. RFI was used for fast IC_{50} determination. For the fluorescence measurements, the median of the RFI was determined from five measuring points within a single well. The error bars show the deviation determined from eight replicates (wells) per dilution. Red object count (ROC) was determined alternatively to confluency and roughness during live cell imaging experiments.

RT-PCR and RT-qPCR Analysis

Severe acute respiratory syndrome coronavirus 2 RNA from cell culture supernatant samples was isolated using AVL buffer and the QIAamp Viral RNA Kit (Qiagen) according to the manufacturer's instructions. Intracellular RNAs were isolated using the RNeasy Mini Kit (Qiagen) as described by the manufacturer. For detection of intracellular and extracellular SARS-CoV-2 genomic RNA, primers and dual-labeled probes were used (**Supplementary Table 2**). Multiplex RT-qPCR assay were carried out using Reliance One-Step Multiplex RT-qPCR Supermix (Bio-Rad) or LightCycler Multiplex RNA Virus Master (Roche). SYBR green based RT-qPCRs were performed using Luna Universal One-Step RT-qPCR Kit (NEB) (Kim et al., 2020; Shin et al., 2020; Wolfel et al., 2020; Kohmer et al., 2021).

Western Blot Analysis

Protein extracts, separated by SDS-PAGE and transferred onto PVDF membranes, were probed with antibodies against FLAG (F1804, Sigma), ACE2 (ab15248, Abcam), or GAPDH (2275-PC-100, Trevigen). Proteins of interest were detected with HRP-conjugated secondary IgG antibody and visualized with ECL Western blotting substrate (Thermo Scientific) according to the provided protocol.

SARS-CoV-2 Neutralization Assay

The mAb solutions were serially diluted 1:2 and incubated with 4000 $TCID_{50}$/ml of each SARS-CoV-2 variant and subjected to cell based SARS-CoV-2 neutralization assay (Widera et al., 2021b). The corresponding sample dilution resulting in 50% virus neutralization titer (NT_{50}) was determined. After 3 days of incubation cells were evaluated for the presence of a CPE. Spike Staining was performed as described below.

Microscopy and Imaging of SARS-CoV-2 Infected Cells

Time-lapse images were taken with the SparkCyto 400 multimode reader with integrated microscope unit (TECAN). The cell culture condition was maintained with the integrated incubation chamber with 5% CO_2 and 37°C. Cells were imaged in regular intervals as indicated. Confluency and roughness measurements were performed with the 10× objective. A single central image was used to record movies showing the CPE (**Supplementary Movies 1–3**). ROC, Confluency and roughness were analyzed using ImageAnalyzer Software v.1.1 (Tecan). Immunofluorescence experiments were performed using SARS-CoV and SARS-CoV-2 Spike antibody (40150-R007, Sino Biologicals) and Alexa-488 conjugated anti-rabbit secondary antibody (Invitrogen).

Statistical Analysis

If not indicated differently all infection experiments were repeated in three independent experiments. Statistical significance compared to untreated control was determined using unpaired Student's t-test. Asterisks indicated p-values as $^*p < 0.05$, $^{**}p \leq 0.01$, and $^{***}p \leq 0.001$.

DATA AVAILABILITY STATEMENT

The original contributions presented in the study are included in the article/**Supplementary Material**, further inquiries can be directed to the corresponding author/s.

AUTHOR CONTRIBUTIONS

MW provided the graphs and figures, drafted and wrote the manuscript, performed viral outgrowth, analyzed the data, and contributed to conception and design of the study. AW wrote sections of the manuscript, performed the infection and live cell imaging experiments, preparative cell culturing, western blotting, and immunofluorescence staining and analyzed the

SUPPLEMENTARY MATERIAL

The Supplementary Material for this article can be found online at: https://www.frontiersin.org/articles/10.3389/fmicb.2021.701198/full#supplementary-material

REFERENCES

Andreakos, E., and Tsiodras, S. (2020). COVID-19: lambda interferon against viral load and hyperinflammation. *EMBO Mol. Med.* 12:e12465.

Belouzard, S., Chu, V. C., and Whittaker, G. R. (2009). Activation of the SARS coronavirus spike protein via sequential proteolytic cleavage at two distinct sites. *Proc. Natl. Acad. Sci. U. S. A.* 106, 5871–5876. doi: 10.1073/pnas.0809524106

Bestle, D., Heindl, M. R., Limburg, H., Van Lam Van, T., Pilgram, O., Moulton, H., et al. (2020). TMPRSS2 and furin are both essential for proteolytic activation of SARS-CoV-2 in human airway cells. *Life Sci. Alliance* 3:e202000786. doi: 10.26508/lsa.202000786

Bojkova, D., Bechtel, M., Mclaughlin, K. M., Mcgreig, J. E., Klann, K., Bellinghausen, C., et al. (2020a). Aprotinin Inhibits SARS-CoV-2 Replication. *Cells* 9:2377. doi: 10.3390/cells9112377

Bojkova, D., Klann, K., Koch, B., Widera, M., Krause, D., Ciesek, S., et al. (2020b). Proteomics of SARS-CoV-2-infected host cells reveals therapy targets. *Nature* 583, 469–472. doi: 10.1038/s41586-020-2332-7

Buchrieser, J., Dufloo, J., Hubert, M., Monel, B., Planas, D., Rajah, M. M., et al. (2020). Syncytia formation by SARS-CoV-2-infected cells. *EMBO J.* 39:e106267.

Bussani, R., Schneider, E., Zentilin, L., Collesi, C., Ali, H., Braga, L., et al. (2020). Persistence of viral RNA, pneumocyte syncytia and thrombosis are hallmarks of advanced COVID-19 pathology. *EBioMedicine* 61:103104. doi: 10.1016/j.ebiom.2020.103104

Chan, J. F., Chan, K. H., Choi, G. K., To, K. K., Tse, H., Cai, J. P., et al. (2013). Differential cell line susceptibility to the emerging novel human betacoronavirus 2c EMC/2012: implications for disease pathogenesis and clinical manifestation. *J. Infect. Dis.* 207, 1743–1752. doi: 10.1093/infdis/jit123

Drosten, C., Gunther, S., Preiser, W., Van Der Werf, S., Brodt, H. R., Becker, S., et al. (2003). Identification of a novel coronavirus in patients with severe acute respiratory syndrome. *N. Engl. J. Med.* 348, 1967–1976.

Garcia-Beltran, W. F., Lam, E. C., St Denis, K., Nitido, A. D., Garcia, Z. H., Hauser, B. M., et al. (2021). Multiple SARS-CoV-2 variants escape neutralization by vaccine-induced humoral immunity. *Cell* 184, 2372–2383.e9.

Giard, D. J., Aaronson, S. A., Todaro, G. J., Arnstein, P., Kersey, J. H., Dosik, H., et al. (1973). In vitro cultivation of human tumors: establishment of cell lines derived from a series of solid tumors. *J. Natl. Cancer Inst.* 51, 1417–1423. doi: 10.1093/jnci/51.5.1417

Greaney, A. J., Loes, A. N., Crawford, K. H. D., Starr, T. N., Malone, K. D., Chu, H. Y., et al. (2021). Comprehensive mapping of mutations to the SARS-CoV-2 receptor-binding domain that affect recognition by polyclonal human serum antibodies. *bioRxiv* [preprint]. doi: 10.1101/2020.12.31.425021

Heuberger, J., Trimpert, J., Vladimirova, D., Goosmann, C., Lin, M., Schmuck, R., et al. (2021). Epithelial response to IFN-gamma promotes SARS-CoV-2 infection. *EMBO Mol. Med.* 13:e13191.

Heurich, A., Hofmann-Winkler, H., Gierer, S., Liepold, T., Jahn, O., and Pohlmann, S. (2014). TMPRSS2 and ADAM17 cleave ACE2 differentially and only proteolysis by TMPRSS2 augments entry driven by the severe acute respiratory syndrome coronavirus spike protein. *J. Virol.* 88, 1293–1307. doi: 10.1128/jvi.02202-13

Hoehl, S., Rabenau, H., Berger, A., Kortenbusch, M., Cinatl, J., Bojkova, D., et al. (2020). Evidence of SARS-CoV-2 Infection in Returning Travelers from Wuhan, China. *N. Engl. J. Med.* 382, 1278–1280. doi: 10.1056/nejmc2001899

Hoffmann, M., Arora, P., Gross, R., Seidel, A., Hornich, B. F., Hahn, A. S., et al. (2021a). SARS-CoV-2 variants B.1.351 and P.1 escape from neutralizing antibodies. *Cell* 184, 2384–2393.e12.

Hoffmann, M., Hofmann-Winkler, H., Smith, J. C., Kruger, N., Arora, P., Sorensen, L. K., et al. (2021b). Camostat mesylate inhibits SARS-CoV-2 activation by TMPRSS2-related proteases and its metabolite GBPA exerts antiviral activity. *EBioMedicine* 65:103255. doi: 10.1016/j.ebiom.2021.103255

Hoffmann, M., Kleine-Weber, H., and Pöhlmann, S. (2020a). A Multibasic Cleavage Site in the Spike Protein of SARS-CoV-2 Is Essential for Infection of Human Lung Cells. *Mol. Cell* 78, 779–784.e5.

Hoffmann, M., Kleine-Weber, H., Schroeder, S., Kruger, N., Herrler, T., Erichsen, S., et al. (2020b). SARS-CoV-2 Cell Entry Depends on ACE2 and TMPRSS2 and Is Blocked by a Clinically Proven Protease Inhibitor. *Cell* 181, 271–280.e8.

Karki, R., Sharma, B. R., Tuladhar, S., Williams, E. P., Zalduondo, L., Samir, P., et al. (2021). Synergism of TNF-alpha and IFN-gamma Triggers Inflammatory Cell Death, Tissue Damage, and Mortality in SARS-CoV-2 Infection and Cytokine Shock Syndromes. *Cell* 184, 149–168.e17.

Keidar, S., Kaplan, M., and Gamliel-Lazarovich, A. (2007). ACE2 of the heart: from angiotensin I to angiotensin (1-7). *Cardiovasc. Res.* 73, 463–469. doi: 10.1016/j.cardiores.2006.09.006

Kim, D., Lee, J. Y., Yang, J. S., Kim, J. W., Kim, V. N., and Chang, H. (2020). The Architecture of SARS-CoV-2 Transcriptome. *Cell* 181, 914–921.e10.

Kohmer, N., Toptan, T., Pallas, C., Karaca, O., Pfeiffer, A., Westhaus, S., et al. (2021). The Comparative Clinical Performance of Four SARS-CoV-2 Rapid Antigen Tests and Their Correlation to Infectivity In Vitro. *J. Clin. Med.* 10:328. doi: 10.3390/jcm10020328

Kowarz, E., Loscher, D., and Marschalek, R. (2015). Optimized Sleeping Beauty transposons rapidly generate stable transgenic cell lines. *Biotechnol. J.* 10, 647–653. doi: 10.1002/biot.201400821

Lan, J., Ge, J., Yu, J., Shan, S., Zhou, H., Fan, S., et al. (2020). Structure of the SARS-CoV-2 spike receptor-binding domain bound to the ACE2 receptor. *Nature* 581, 215–220.

Lavender, K. J., Gibbert, K., Peterson, K. E., Van Dis, E., Francois, S., Woods, T., et al. (2016). Interferon Alpha Subtype-Specific Suppression of HIV-1 Infection In Vivo. *J. Virol.* 90, 6001–6013. doi: 10.1128/jvi.00451-16

Lea, T. (2015). "Caco-2 Cell Line," in *The Impact Of Food Bioactives On Health: In Vitro And Ex Vivo Models*, eds K. Verhoeckx, P. Cotter, I. Lopez-Exposito, C. Kleiveland, T. Lea, A. Mackie, et al. (Cham CH: Springer), 103–111. doi: 10.1007/978-3-319-16104-4_10

Li, W., Moore, M. J., Vasilieva, N., Sui, J., Wong, S. K., Berne, M. A., et al. (2003). Angiotensin-converting enzyme 2 is a functional receptor for the SARS coronavirus. *Nature* 426, 450–454.

Li, Y., Renner, D. M., Comar, C. E., Whelan, J. N., Reyes, H. M., Cardenas-Diaz, F. L., et al. (2021). SARS-CoV-2 induces double-stranded RNA-mediated innate immune responses in respiratory epithelial-derived cells and cardiomyocytes. *Proc. Natl. Acad. Sci. U. S. A.* 118:e2022643118. doi: 10.1073/pnas.2022643118

Matsuyama, S., Nagata, N., Shirato, K., Kawase, M., Takeda, M., and Taguchi, F. (2010). Efficient activation of the severe acute respiratory syndrome coronavirus spike protein by the transmembrane protease TMPRSS2. *J. Virol.* 84, 12658–12664. doi: 10.1128/jvi.01542-10

Matsuyama, S., Nao, N., Shirato, K., Kawase, M., Saito, S., Takayama, I., et al. (2020). Enhanced isolation of SARS-CoV-2 by TMPRSS2-expressing cells. *Proc. Natl. Acad. Sci.* 117, 7001–7003. doi: 10.1073/pnas.2002589117

McKinney, C. A., Fattah, C., Loughrey, C. M., Milligan, G., and Nicklin, S. A. (2014). Angiotensin-(1-7) and angiotensin-(1-9): function in cardiac and vascular remodelling. *Clin. Sci.* 126, 815–827. doi: 10.1042/cs20130436

Ogando, N. S., Dalebout, T. J., Zevenhoven-Dobbe, J. C., Limpens, R. W. A. L., van der Meer, Y., Caly, L., et al. (2020). SARS-coronavirus-2 replication in Vero E6 cells: replication kinetics, rapid adaptation and cytopathology. *J. Gen. Virol.* 101, 925–940. doi: 10.1099/jgv.001453

Osada, N., Kohara, A., Yamaji, T., Hirayama, N., Kasai, F., Sekizuka, T., et al. (2014). The genome landscape of the african green monkey kidney-derived vero cell line. *DNA Res.* 21, 673–683. doi: 10.1093/dnares/dsu029

Qian, Z., Dominguez, S. R., and Holmes, K. V. (2013). Role of the spike glycoprotein of human Middle East respiratory syndrome coronavirus (MERS-CoV) in virus entry and syncytia formation. *PLoS One* 8:e76469. doi: 10.1371/journal.pone.0076469

Rahman, N., Basharat, Z., Yousuf, M., Castaldo, G., Rastrelli, L., and Khan, H. (2020). Virtual Screening of Natural Products against Type II Transmembrane Serine Protease (TMPRSS2), the Priming Agent of Coronavirus 2 (SARS-CoV-2). *Molecules* 25:2271. doi: 10.3390/molecules25102271

Shang, J., Wan, Y., Luo, C., Ye, G., Geng, Q., Auerbach, A., et al. (2020). Cell entry mechanisms of SARS-CoV-2. *Proc. Natl. Acad. Sci. U. S. A.* 117, 11727–11734.

Shin, D., Mukherjee, R., Grewe, D., Bojkova, D., Baek, K., and Bhattacharya, A. (2020). Papain-like protease regulates SARS-CoV-2 viral spread and innate immunity. *Nature* 587, 657–662. doi: 10.1038/s41586-020-2601-5

Skipper, K. A., Andersen, P. R., Sharma, N., and Mikkelsen, J. G. (2013). DNA transposon-based gene vehicles - scenes from an evolutionary drive. *J. Biomed. Sci.* 20:92. doi: 10.1186/1423-0127-20-92

Stanifer, M. L., Kee, C., Cortese, M., Zumaran, C. M., Triana, S., Mukenhirn, M., et al. (2020). Critical Role of Type III Interferon in Controlling SARS-CoV-2 Infection in Human Intestinal Epithelial Cells. *Cell Rep.* 32:107863. doi: 10.1016/j.celrep.2020.107863

Starr, T. N., Greaney, A. J., Hilton, S. K., Ellis, D., Crawford, K. H. D., Dingens, A. S., et al. (2020). Deep Mutational Scanning of SARS-CoV-2 Receptor Binding Domain Reveals Constraints on Folding and ACE2 Binding. *Cell* 182, 1295–1310.e20.

Takayama, K. (2020). In Vitro and Animal Models for SARS-CoV-2 research. *Trends Pharmacol. Sci.* 41, 513–517. doi: 10.1016/j.tips.2020.05.005

Toptan, T., Hoehl, S., Westhaus, S., Bojkova, D., Berger, A., Rotter, B., et al. (2020). Optimized qRT-PCR Approach for the Detection of Intra- and Extra-Cellular SARS-CoV-2 RNAs. *Int. J. Mol. Sci.* 21:4396. doi: 10.3390/ijms21124396

Torvinen, M., Campwala, H., and Kilty, I. (2007). The role of IFN-gamma in regulation of IFN-gamma-inducible protein 10 (IP-10) expression in lung epithelial cell and peripheral blood mononuclear cell co-cultures. *Respir. Res.* 8:80.

Wang, M., Cao, R., Zhang, L., Yang, X., Liu, J., Xu, M., et al. (2020). Remdesivir and chloroquine effectively inhibit the recently emerged novel coronavirus (2019-nCoV) in vitro. *Cell Res.* 30, 269–271. doi: 10.1038/s41422-020-0282-0

Wang, Q., Zhang, Y., Wu, L., Niu, S., Song, C., Zhang, Z., et al. (2020). Structural and Functional Basis of SARS-CoV-2 Entry by Using Human ACE2. *Cell* 181, 894–904.e9.

Westhaus, S., Widera, M., Rabenau, H. F., Hoehl, S., Bojkova, D., Cinatl, J., et al. (2020). Evaluation of stability and inactivation methods of SARS-CoV-2 in context of laboratory settings. *bioRxiv* [preprint]. doi: 10.1101/2020.09.11.292581

Widera, M., Muhlemann, B., Corman, V. M., Toptan, T., Beheim-Schwarzbach, J., Kohmer, N., et al. (2021a). Surveillance of SARS-CoV-2 in Frankfurt am Main from October to December 2020 Reveals High Viral Diversity Including Spike Mutation N501Y in B.1.1.70 and B.1.1.7. *Microorganisms* 9:748. doi: 10.3390/microorganisms9040748

Widera, M., Wilhelm, A., Hoehl, S., Pallas, C., Kohmer, N., Wolf, T., et al. (2021b). Bamlanivimab does not neutralize two SARS-CoV-2 variants carrying E484K in vitro. *medRxiv* [preprint]. doi: 10.1101/2021.02.24.21252372

Wolfel, R., Corman, V. M., Guggemos, W., Seilmaier, M., Zange, S., Muller, M. A., et al. (2020). Virological assessment of hospitalized patients with COVID-2019. *Nature* 581, 465–469. doi: 10.1038/s41586-020-2196-x

World Health Organisation [WHO] (2021). "Covid-19 Weekly Epidemiological Update On Covid-19", In: Report On Coronavirus Disease 2019 (Covid-19), 44 Edn. Geneva: World Health Organisation.

Zhu, N., Zhang, D., Wang, W., Li, X., Yang, B., and Song, J. (2020). A Novel Coronavirus from Patients with Pneumonia in China, 2019. *N. Engl. J. Med.* 382, 727–733.

Conflict of Interest: The authors declare that the research was conducted in the absence of any commercial or financial relationships that could be construed as a potential conflict of interest.

Publisher's Note: All claims expressed in this article are solely those of the authors and do not necessarily represent those of their affiliated organizations, or those of the publisher, the editors and the reviewers. Any product that may be evaluated in this article, or claim that may be made by its manufacturer, is not guaranteed or endorsed by the publisher.